Optics Letters

# Near-complete violation of Kirchhoff's law of thermal radiation with a 0.3 T magnetic field

Bo Zhao,[1,3,*] Yu Shi,[1] Jiahui Wang,[2] Zhexin Zhao,[1] Nathan Zhao,[2] and Shanhui Fan[1,3,4]

[1]Department of Electrical Engineering, Stanford University, Stanford, California 94305, USA
[2]Department of Applied Physics, Stanford University, Stanford, California 94305, USA
[3]Ginzton Laboratory, Stanford University, Stanford, California 94305, USA
[4]e-mail: shanhui@stanford.edu
*Corresponding author: bzhao89@stanford.edu

Received 21 June 2019; revised 26 July 2019; accepted 26 July 2019; posted 30 July 2019 (Doc. ID 370715); published 22 August 2019

**The capability to overcome Kirchhoff's law of thermal radiation provides new opportunities in energy harvesting and thermal radiation control. Previously, design towards demonstrating such capability requires a magnetic field of 3 T, which is difficult to achieve in practice. In this work, we propose a nanophotonic design that can achieve such capability with a far more modest magnetic field of 0.3 Tesla, a level that can be achieved with permanent magnets. Our design uses guided resonance in low-loss dielectric gratings sitting on a magneto-optical material, which provides significant enhancement on the sensitivity to the external magnetic field.** © 2019 Optical Society of America

https://doi.org/10.1364/OL.44.004203

The vast majority of thermal emitters obey Kirchhoff's law, which states that, for a given frequency and direction, spectral-directional emissivity $\varepsilon$ is equal to spectral-directional absorptivity $\alpha$ for both transverse electric and transverse magnetic (TM) polarizations [1–5]. Kirchhoff's law is a consequence of the Lorentz reciprocity theorem of Maxwell's equations [6,7]. For nonreciprocal emitters, for example, emitters containing magneto-optical materials that are described by asymmetric dielectric tensors, Kirchhoff's law no longer holds, and spectral-directional emissivity and absorptivity can be different [8–11]. Nonreciprocal thermal emitters provide new capabilities for managing photon heat flow and can be used to fundamentally improve the efficiency of energy harvesting systems [12–16].

Despite their significant potential in applications, there have not been many designs of nonreciprocal thermal emitters. Recently, Zhu and Fan [9] proposed a design using a photonic crystal made of magneto-optical materials (InAs) [Fig. 1(b)]. This design can achieve near-complete violation of Kirchhoff's law, i.e., the difference between the emissivity and absorptivity at a given frequency and direction can reach near unity. However, due to the weak magnetic response of the materials in the infrared range, the structure requires a magnetic field with strength of 3 T. Such a strong magnetic field typically requires electromagnets with superconducting coils [17]. For practical applications, it would be much more attractive if the required magnetic field can be significantly reduced.

In this Letter, we propose a nanophotonic design of thermal emitters [Fig. 1(a)] that can achieve near-complete violation of Kirchhoff's law but only requires magnetic fields on the order of 0.1 T. Such a magnetic field can be achieved with permanent magnets such as neodymium magnets [17]. Instead of using InAs as the photonic crystal material, our design uses a photonic crystal made of a low-loss dielectric material, electromagnetically coupled with an InAs film that provides the nonreciprocal effect. The whole structure, therefore, can support narrow-bandwidth nonreciprocal waveguide resonances that are very sensitive to the change of the external magnetic field.

Both designs in Fig. 1 are grating structures that possess a periodic array of strips with the periodicity along the $x$ direction. The period is $\Lambda$, and the width of the strips is $w$. The values of all geometrical parameters are provided in the figure caption. In these designs, reciprocity is broken using the magneto-optical response of InAs. Consider TM polarization with an electric field in the $x$–$y$ plane. In Voigt geometry [18,19], an external magnetic field (blue arrow the figure) is applied in the $z$ direction. The permittivity tensor of InAs in the presence of such a $B$ field is [9,20]

$$\bar{\bar{\varepsilon}} = \begin{bmatrix} \varepsilon_{xx} & \varepsilon_{xy} & 0 \\ \varepsilon_{yx} & \varepsilon_{yy} & 0 \\ 0 & 0 & \varepsilon_{zz} \end{bmatrix}, \tag{1}$$

where

$$\varepsilon_{xx} = \varepsilon_{yy} = \varepsilon_\infty - \frac{\omega_p^2(\omega + i\Gamma)}{\omega[(\omega + i\Gamma)^2 - \omega_c^2]}, \tag{2}$$

$$\varepsilon_{xy} = -\varepsilon_{yx} = i\frac{\omega_p^2\omega_c}{\omega[(\omega + i\Gamma)^2 - \omega_c^2]}, \tag{3}$$

$$\varepsilon_{zz} = \varepsilon_\infty - \frac{\omega_p^2}{\omega(\omega + i\Gamma)}. \tag{4}$$

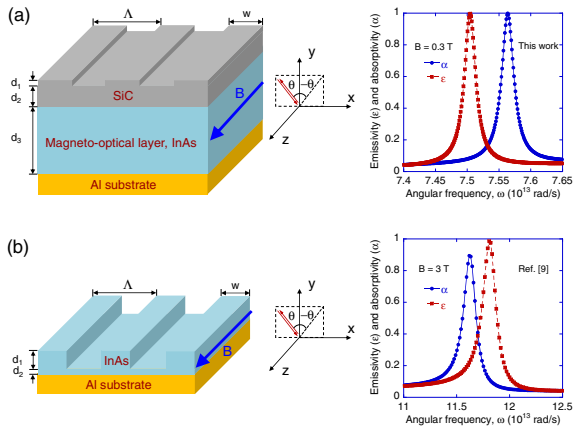


**Fig. 1.** (a) Schematic of the proposed structure for the violation of Kirchhoff's law. The structure consists of (from top to bottom) a SiC grating, a magneto-optical film made of InAs, and an Al substrate. Throughout the study, we fix the parameters as $\Lambda = 10$ μm, $w = 5$ μm, $d_1 = 0.3$ μm, $d_2 = 4$ μm, and $d_3 = 20$ μm. An external magnetic field is applied in the $z$ direction. The incident wave is TM polarized with an electric field in the $x$–$y$ plane. The incidence angle is $\theta$. The two arrows on the $x$–$y$–$z$ coordinate indicate the absorption and emission processes. The right panel shows the emissivity and absorptivity of the structure under a 0.3 T $B$ field for $\theta = 65°$. (b) Schematic of the structure design in Ref. [9]. The structure consists of an InAs grating atop an Al substrate. The geometric parameters are $\Lambda = 7.24$ μm, $w = 3.2$ μm, $d_1 = 1.981$ μm, $d_2 = 0.485$ μm. An external magnetic field is applied in the $z$ direction. The right panel shows the emissivity and absorptivity of the structure under a 3 T $B$ field for the direction with $\theta = 61.28°$.

In Eqs. (2)–(4), $\varepsilon_\infty = 12.37$ is the high-frequency permittivity, $\Gamma$ is the relaxation rate, $\omega_p = \sqrt{n_e e^2/(m^* \varepsilon_0)}$ is the plasma frequency, and $\omega_c = eB/m^*$ is the cyclotron frequency. Here, $n_e$ is the free electron carrier density, $m*$ is the effective electron mass, $B$ is the external magnetic field, and $\varepsilon_0$ is the vacuum permittivity. In this work, we assume $n_e = 7.8 \times 10^{17}$ cm$^{-3}$ and $m^* = 0.033 m_e$ ($m_e$ is the electron mass), and a constant relaxation rate $\Gamma = 1.55 \times 10^{11}$ rad/s given by the model provided in Ref. [9] for the wavelength range considered in this work. This doping level is much higher than the intrinsic carrier concentration, even at elevated temperatures. Thus, we expect the Drude model to hold true for high temperatures as well. The effect of Landau-level quantization is not significant since at room temperature $T$, which is the focus of this study, $k_B T \gg \hbar\omega_c$ [21]. From Eq. (3), reciprocity is broken since $\varepsilon_{xy} \neq \varepsilon_{yx}$. The magneto-optical effect of InAs becomes stronger when the ratio between the off-diagonal component and the diagonal component, i.e., $|\varepsilon_{xy}|/|\varepsilon_{xx}|$, becomes larger [22]. Both structures in Fig. 1 use Al as the substrate. The permittivity of Al is described by a Drude model that is identical to the form given in Eq. (4), with parameters [23] $\varepsilon_\infty = 1$, $\omega_p = 2.24 \times 10^{16}$ rad/s, and $\Gamma = 1.24 \times 10^{14}$ rad/s. The substrate is optically thick.

For the structures in Fig. 1, with a proper choice of periodicity $\Lambda$, there is only specular reflection in the wavelength range of interest. Incoming waves from a channel in air with an angle of incidence $\theta$ will be either absorbed by the structure, resulting in an absorptivity $\alpha_\theta$, or reflected to the complementary channel in the $-\theta$ direction, resulting in the reflectivity $R_\theta$. From energy conservation, $\alpha_\theta = 1 - R_\theta$. The emissivity $\varepsilon_\theta$ to the channel $\theta$, on the other hand, is related to the reflectivity in the complementary channel by $\varepsilon_\theta = 1 - R_{-\theta}$, as can be derived using the thermodynamic argument detailed in Ref. [9]. For nonreciprocal structures, $R_\theta \neq R_{-\theta}$ [24–26]; thus, $\alpha_\theta \neq \varepsilon_\theta$, and Kirchhoff's law is violated. The thermodynamic consideration above also allows us to determine the absorptivity and emissivity from reflectivity calculations.

From the discussion above, to achieve a strong violation of Kirchhoff's law, one needs to maximize the contrast between $R_\theta$ and $R_{-\theta}$. In the design of Ref. [9] [Fig. 1(b)], this is achieved by exploiting guided resonance in the InAs layer. A uniform InAs layer supports the guided mode. In the presence of the grating, some of the guided mode can coupled to free space radiation to create guided resonance [27]. With the proper choice of grating parameters, the guided mode can be critically coupled to an incident wave and results in perfect absorption and emission. For the structure in Fig. 1(b), in the absence of the magnetic field, the grating was designed to critically couple to the plane wave from the direction in $\theta = 61.28°$ at $\omega = 11.8 \times 10^{13}$ rad/s (15.96 μm). In the presence of the magnetic field, the band structure of the guided resonance is no longer symmetric, i.e., $\omega(k_x) \neq \omega(-k_x)$, where $k_x$ is the wavevector along the $x$ direction. Since incident waves from channels $\theta$ and $-\theta$ couple to resonance at $k_x$ and $-k_x$, respectively, the asymmetry in the band structure results in $R_\theta \neq R_{-\theta}$. Hence, we observe the difference between the emissivity and absorptivity, as shown in Fig. 1(b). At the emissivity peak, the difference between the absorptivity and emissivity reaches about 0.95, indicating a near-complete violation of Kirchhoff's law. However, because InAs is lossy in the designed frequency range ($\varepsilon_{xx} = 6.9 + 0.1i$ at the resonance frequency), the quality ($Q$) factor of the guided resonance, as measured by the ratio between the resonant frequency and resonant linewidth in the emissivity or absorptivity spectra, is about 76, which is relatively modest. Thus, the applied magnetic field must be sufficiently strong (i.e., $B = 3$ T in order to achieve $\varepsilon_{xy} \approx 0.75i$ at the resonance frequency) such that the resonance peaks in the absorptivity and the emissivity can be separated from one another. We note that the maximum value of difference between emissivity and absorptivity in the wavelength range considered here is linearly dependent on the magnitude of the $B$ field on the small-$B$ limit. Therefore, to quantify the dependence of the strength of Kirchhoff's law violation on the magnetic field, we define sensitivity as

$$\xi(\theta, \omega) = \frac{|\alpha(\theta, \omega) - \varepsilon(\theta, \omega)|}{B}. \tag{5}$$

A larger $\xi$ indicates a stronger violation of Kirchhoff's law for a given magnetic field. For the emitter discussed above, the maximum value of $\xi$ is about $0.31/T$.

In order to reduce the required magnetic field, it is therefore important to create a guided resonance with a higher $Q$ factor, while maintaining the strength of the magneto-optical effects on the guided resonance. In our design in Fig. 1(a), we consider instead a SiC grating on top of a uniform InAs film. The permittivity of SiC can be described by a Lorentz model [5], $\varepsilon_{\mathrm{SiC}} = \varepsilon_{\infty,\mathrm{SiC}}[1 + (\omega_{\mathrm{LO}}^2 - \omega_{\mathrm{TO}}^2)/(\omega_{\mathrm{TO}}^2 - i\gamma\omega - \omega^2)]$, where $\varepsilon_{\infty,\mathrm{SiC}} = 6.7$, $\omega_{\mathrm{LO}} = 1.83 \times 10^{14}$ rad/s, $\omega_{\mathrm{TO}} = 1.49 \times 10^{14}$ rad/s, and $\gamma = 8.97 \times 10^{11}$ rad/s. Near the operating

frequency $\omega_0 = 7.50 \times 10^{13}$ rad/s, SiC has very low material loss ($\varepsilon_{\mathrm{SiC}} = 11.13 + 0.018i$). With the appropriate choice of the grating parameters, the structure can support a critically coupled resonance near $\omega_0$ for incident light with $\theta = 65°$. This resonance possesses a $Q$ factor of 312, which is significantly higher as compared to the structure in Fig. 1(b). While in this structure, the field is concentrated in the SiC layer; since the InAs layer is immediately adjacent, there are significant field components inside the InAs layer. In addition, near $\omega_0$ the real part of $\varepsilon_{xx}$ for InAs crosses zero, and the magneto-optical effect is further enhanced [28] since the strength of the magneto-optical effect is related to $|\varepsilon_{xy}|/|\varepsilon_{xx}|$. Combining the effects of increasing $Q$ and enhancing the magneto-optical effect, in our design of Fig. 1(a), with a modest field $B = 0.3$ T, the emissivity and absorptivity peaks have very little overlap, and we obtain a frequency region between the peaks with near-complete violation of Kirchhoff's law, as shown in Fig. 1(a). The applied magnetic field of 0.3 T is within the range that can be achieved with permanent magnets. For example, neodymium magnets can create a magnetic field up to about 1 T [17]. The maximum value of $\xi$ reaches 3.1/T, which is one order of magnitude higher than that of the emitter in Fig. 1(b).

In Fig. 2 we show the $x$ component of the electric fields at the frequencies $\omega_e = 7.50 \times 10^{13}$ rad/s (25.11 μm) and $\omega_a = 7.56 \times 10^{13}$ rad/s (24.92 μm). These two frequencies correspond to the emissivity or absorptivity peaks in Fig. 1(a) for light emitting to or incident from the channel at $\theta = 65°$. For both frequencies, we plot field patterns as excited by light with angles of incidence of $\theta = \pm 65°$. We use the finite-difference frequency-domain technique with the total-field scattered-field formalism. The dashed lines indicate the position of the line source used to excite the incident wave. The field pattern above the dashed line contains only the reflected field. At $\omega = \omega_e$, for $\theta = 65°$ [Fig. 2(a)], the incident wave does not significantly excite a guided resonance, and instead most of the incident power is reflected, resulting in a low absorptivity. In contrast, at the same frequency, when the incident wave is illuminated from $\theta = -65°$ [Fig. 2(b)], the incident wave is strongly coupled to the guided resonance, and the reflection is almost completely absent. The contrast between Figs. 2(a) and 2(b) in the reflection is related to the strong emissivity peak to the channel at $\theta = 65°$. On the other hand, at $\omega = \omega_a$, the incidence wave from $\theta = 65°$ is strongly coupled to the guided resonance and is totally absorbed [Fig. 2(c)], consistent with the presence of the absorptivity peak at this frequency. The incident wave from $\theta = -65°$ is strongly reflected. The field patterns here provide visualization that the guided resonance has an asymmetrical dispersion relation $\omega(k_x) \neq \omega(-k_x)$, which underlies the violation of Kirchhoff's law.

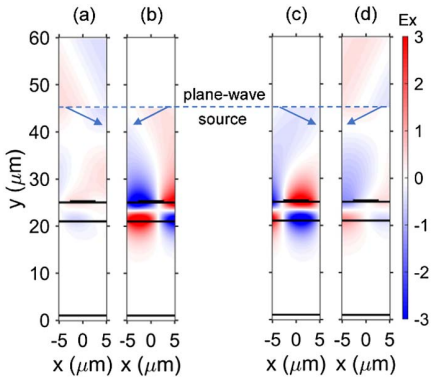


**Fig. 2.** Electric field ($E_x$) at (left panel) peak-emissivity frequency ($\omega = 7.50 \times 10^{13}$ rad/s) and (right panel) peak-absorptivity frequency ($\omega = 7.56 \times 10^{13}$ rad/s). The dashed horizontal line shows the location of the plane-wave source, above which the field only contains the reflected field. The incident direction of the plane wave, $\theta = 65°$ [in (a) and (c)] or $\theta = -65°$ [in (b) and (d)], are indicated using an arrow on each field plot. The magnitude of the incident electric field is set to unity.

The nonreciprocal behavior of the guided resonance dispersion relation for the proposed structure in Fig. 1(a) can be quantitatively understood by first considering the dispersion relation $\omega(k_x)$ of the fundamental guided mode of a corresponding uniform SiC slab atop a semi-infinite InAs region, which can be obtained by solving [29]

$$\tan(k_{y,\mathrm{SiC}} t) = \frac{k_{y,\mathrm{SiC}} \varepsilon_{\mathrm{SiC}} [k_{y,\mathrm{air}} - i\xi_{yx} k_x + k_{y,\mathrm{InAs}} \xi_{xx}]}{k_{y,\mathrm{SiC}}^2 + \varepsilon_{\mathrm{SiC}}^2 k_{y,\mathrm{air}} [i\xi_{yx} k_x - k_{y,\mathrm{InAs}} \xi_{xx}]}. \quad \textbf{(6)}$$

Here, $t = d_1/2 + d_2$ is the thickness of the uniform slab, $\xi_{xx} = \mathrm{Re}(\varepsilon_{xx})/[\mathrm{Re}(\varepsilon_{xx})^2 - \mathrm{Im}(\varepsilon_{xy})^2]$, $\xi_{yx} = i\mathrm{Im}(\varepsilon_{xy})/[\mathrm{Re}(\varepsilon_{xx})^2 - \mathrm{Im}(\varepsilon_{xy})^2]$, $k_{y,\mathrm{air}} = \sqrt{k_x^2 - (\omega/c)^2}$, $k_{y,\mathrm{SiC}} = \sqrt{\mathrm{Re}(\varepsilon_{\mathrm{SiC}})(\omega/c)^2 - k_x^2}$, and $k_{y,\mathrm{InAs}} = \sqrt{k_x^2 - (\omega/c)^2/\xi_{xx}}$ are the $y$ components of the wavevectors in the air, SiC, and InAs regions, respectively. When $B \neq 0$ and hence $\xi_{yx} \neq 0$, Eq. (6) indicates that $\omega(k_x) \neq \omega(-k_x)$. When the grating is introduced, part of the dispersion relation gets folded above the light line, resulting in the creation of guided resonance [27]. As an illustration, we plot the absorptivity as a function of frequency and angle of incidence with and without the $B$ field in Figs. 3(a) and 3(b), respectively. The folded dispersion relation from Eq. (6) agrees excellently with the position of the absorptivity peaks. When $B = 0$ T, the dispersion relation is symmetric with respect to $\theta \to -\theta$. With $B \neq 0$ T [Fig. 3(b)], the band at $\theta < 0°$ shifts downward, and the band at $\theta > 0°$ shifts upward, as compared to the bands in Fig. 3(a). As a result, in the frequency range from $7.45 \times 10^{13}$ rad/s to $7.5 \times 10^{13}$ rad/s, the guided resonance exists only for $\theta < 0°$. The violation of Kirchhoff's law is particularly strong in this frequency range. Meanwhile, in this frequency range, the

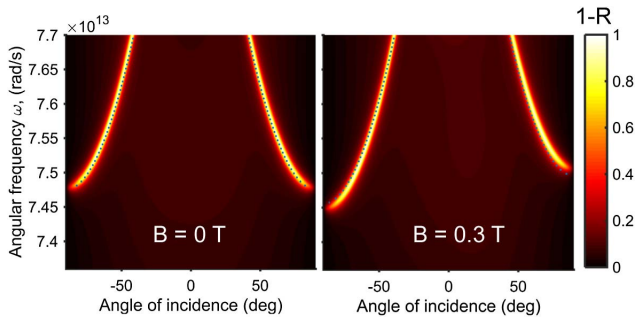


**Fig. 3.** Absorptivity as a function of frequency and angle of incidence for the structure shown in Fig. 1(a) for (a) $B = 0$ T and (b) $B = 0.3$ T. The dotted lines are the analytical solution of the dispersion of the guided resonance given by Eq. (6).

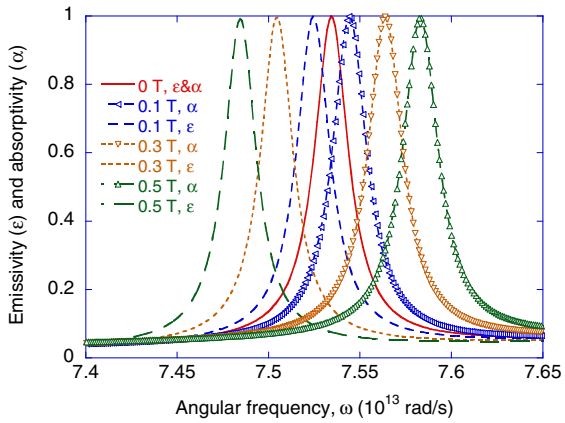


**Fig. 4.** Absorptivity and emissivity spectrum with different magnetic fields at $\theta = 65°$. When $B = 0$ T (the solid red line), the two spectra overlap.

emissivity and absorptivity are quite different in a wide angular range of $50° < |\theta| < 90°$.

The degree for which Kirchhoff's law is violated depends on the strength of the magnetic field. Figure 4 shows the emissivity and absorptivity spectra under different $B$ fields at $\theta = 65°$. The emissivity and absorptivity peaks become more separated as the $B$ field increases. At $B = 0.1$ T, the separation between the absorptivity and emissivity peaks starts to exceed the linewidth of the peaks. Thus, one can observe strong violation of Kirchhoff's law, even for a magnetic field as low as 0.1 T in our structure. The results here also indicate that the use of the magnetic field can provide a mechanism to tune thermal emissivity. To achieve a given contrast in the absorptivity and emissivity, the required magnetic field can be further reduced with the use of a resonance with a higher $Q$ factor, or by considering coupled resonances. The separation between the frequencies of absorptivity and emissivity peaks increase with the magnetic field. In our structure, the separation saturates at a magnetic field above 1 T, due to the permittivity changes as the frequency shifts.

In conclusion, we propose a photonic crystal design that can achieve near-complete violation of Kirchhoff's law with magnetic field strengths weak enough to be obtained from permanent magnets. The violation of Kirchhoff's law persists over a wide angular range and can be tuned with the applied magnetic field. Our design may pave the way to constructing nonreciprocal thermal emitters of practical interests.

**Funding.** Defense Advanced Research Projects Agency (HR00111820046); U.S. Department of Energy (DE-SC0019140).

**Acknowledgment.** Z. Z. acknowledges the support of a Stanford Graduate Fellowship. B. Z. thanks Dr. Linxiao Zhu for discussions.

## REFERENCES

1. G. Kirchhoff, Annalen der Physik **185**, 275 (1860).
2. M. Planck, *The Theory of Heat Radiation* (Forgotten Books, 2013).
3. J. R. Howell, M. P. Menguc, and R. Siegel, *Thermal Radiation Heat Transfer*, 6th ed. (CRC Press, 2015).
4. T. L. Bergman, A. S. Lavine, F. P. Incropera, and D. P. DeWitt, *Fundamentals of Heat and Mass Transfer* (Wiley, 2017).
5. Z. M. Zhang, *Nano/Microscale Heat Transfer* (McGraw-Hill, 2007).
6. L. D. Landau, E. M. Lifshitz, and L. P. Pitaevskii, *Electrodynamics of Continuous Media*, 2nd ed. (Pergamon, 1984).
7. S. E. Han, Phys. Rev. B **80**, 155108 (2009).
8. W. C. Snyder, Z. Wan, and X. Li, Appl. Opt. **37**, 3464 (1998).
9. L. Zhu and S. Fan, Phys. Rev. B **90**, 220301 (2014).
10. D. A. B. Miller, L. Zhu, and S. Fan, Proc. Natl. Acad. Sci. USA **114**, 4336 (2017).
11. L. Zhu and S. Fan, Phys. Rev. Lett. **117**, 134303 (2016).
12. H. Ries, Appl. Phys. B **32**, 153 (1983).
13. M. A. Green, Nano Lett. **12**, 5985 (2012).
14. Y. Hadad, J. C. Soric, and A. Alu, Proc. Natl. Acad. Sci. **113**, 3471 (2016).
15. A. Polman and H. A. Atwater, Nat. Mater. **11**, 174 (2012).
16. S. Buddhiraju and S. Fan, Phys. Rev. B **96**, 035304 (2017).
17. E. P. Furlani, *Permanent Magnet and Electromechanical Devices* (Academic, 2001).
18. P. S. Pershan, J. Appl. Phys. **38**, 1482 (1967).
19. G. C. Aers and A. D. Boardman, J. Phys. C **11**, 945 (1978).
20. O. Madelung, *Semiconductors: Data Handbook* (Springer, 2004).
21. X.-G. Wen, *Quantum Field Theory of Many-Body Systems* (Oxford University, 2004).
22. X. Luo, M. Zhou, J. Liu, T. Qiu, and Z. Yu, Appl. Phys. Lett. **108**, 131104 (2016).
23. M. A. Ordal, R. J. Bell, R. W. Alexander, L. L. Long, and M. R. Querry, Appl. Opt. **24**, 4493 (1985).
24. Z. Yu, Z. Wang, and S. Fan, Appl. Phys. Lett. **90**, 121133 (2007).
25. M. Vanwolleghem, X. Checoury, W. Śmigaj, B. Gralak, L. Magdenko, K. Postava, B. Dagens, P. Beauvillain, and J.-M. Lourtioz, Phys. Rev. B **80**, 121102 (2009).
26. Z. Zhao, C. Guo, and S. Fan, Phys. Rev. A **99**, 033839 (2019).
27. S. Fan and J. D. Joannopoulos, Phys. Rev. B **65**, 235112 (2002).
28. A. R. Davoyan and N. Engheta, ACS Photon. **6**, 581 (2019).
29. L. Alcantara, *Electromagnetic Materials* (IntechOpen, 2018).